Journal Pre-proof

Adsorption-attraction electrolyte addressing anion-deficient interface for lithium metal batteries

Pengbin Lai, Yaqi Zhang, Junhao Wang, Minghui chen, Xinyu Li, Xiaodie Deng, Qichen Chen, Boyang Huang, Chaolun Gan, Yeguo Zou, Yu Qiao, Peng Zhang, Jinbao Zhao

Please cite this article as: P. Lai, Y. Zhang, J. Wang, M. chen, X. Li, X. Deng, Q. Chen, B. Huang, C. Gan, Y. Zou, Y. Qiao, P. Zhang, J. Zhao, Adsorption-attraction electrolyte addressing anion-deficient interface for lithium metal batteries, *eScience*, https://doi.org/10.1016/j.esci.2025.100399.

This is a PDF file of an article that has undergone enhancements after acceptance, such as the addition of a cover page and metadata, and formatting for readability, but it is not yet the definitive version of record. This version will undergo additional copyediting, typesetting and review before it is published in its final form, but we are providing this version to give early visibility of the article. Please note that, during the production process, errors may be discovered which could affect the content, and all legal disclaimers that apply to the journal pertain.

Adsorption-attraction electrolyte addressing anion-deficient interface for lithium metal batteries

Pengbin Lai[a] [†], *Yaqi Zhang*[a] [†], *Junhao Wang*[a], *Minghui chen*[a], *Xinyu Li*[b], *Xiaodie Deng*[a], *Qichen Chen*[b], *Boyang Huang*[a], *Chaolun Gan*[c], *Yeguo Zou*[a], *Yu Qiao*[a], *Peng Zhang*[*b] and *Jinbao Zhao*[*a]

[a] State-Province Joint Engineering Laboratory of Power Source Technology for New Energy Vehicle, Engineering Research Center of Electrochemical Technology, Ministry of Education, College of Chemistry and Chemical Engineering, Xiamen University, Xiamen 361005, China

[b] College of Energy, Xiamen University, Xiamen 361102, China

[c] Zhangjiagang Guotai Huarong Chemical New Material Co., Ltd, Zhangjiagang 215634, China

* Corresponding Author

E-mail address: pengzhang@xmu.edu.cn (Peng Zhang), jbzhao@xmu.edu.cn (Jinbao Zhao)

[†] *These authors contributed equally to this work*

Abstract

Constructing an optimal solid–electrolyte interphase (SEI) through electrolyte strategies is an effective approach to suppress lithium dendrites and improve deposition/stripping reversibility. Specifically, increasing the proportion of anion coordination in the inner Li^+ solvation sheath promotes the formation of an anion-derived SEI that features a high content of inorganic components favoring Li^+ diffusion. However, whether this anion-rich structure can persist during cycling has not been dynamically investigated. In this work, we not only construct a favorable solvation structure but also study its evolution in both bulk and interface regions across varying temperatures. Additionally, we employ the unique "adsorption-attraction" mechanism of trifluoromethoxybenzene (PhOCF$_3$) solvent to inhibit the undesirable transition from an "anion-rich" to "anion-deficient" structure at the anode interface, which is confirmed by 2D NMR and *in situ* infrared spectroscopy. In summary, this work explores the solvation structure in depth and proposes new perspectives on designing electrolytes for lithium metal batteries.

Keywords

Solvation structure; *In situ* characterization; Lithium metal battery; Low temperature; Localized high-concentration electrolyte

1. Introduction

The lithium metal anode (LMA) enjoys a great reputation for having the highest theoretical capacity (3860 mAh g^{-1}) and lowest redox potential (–3.04 V vs. the standard hydrogen electrode)[1]. However, the high reactivity and tricky plating/stripping process of lithium metal lead to excessive electrolyte consumption and the issue of Li dendrites[2, 3]. To mitigate these challenges, researchers urgently need to design electrolytes for building suitable solid–electrolyte interphases (SEIs).

To realize practical lithium metal batteries (LMBs), multiple electrolyte strategies have been proposed, such as high-concentration electrolytes[4] (HCEs), localized high-concentration electrolytes[5] (LHCEs), and weakly solvating electrolytes[6] (WSEs). The design principle underpinning these strategies is to increase the proportion of contact ion pairs (CIPs) and aggregates (AGGs) in the solvation structure, thereby creating an anion-rich inner sheath. This solution structure not only facilitates the formation of an anion-derived SEI with low interfacial resistance but also promotes the desolvation process[7, 8]. However, the actual solvation structure at the interface will change during the electrochemical process. In particular, when solvated Li^+ enters the electric double layer, the anions will be repelled by the electric field. The subsequent desolvation process at the interface will also lead to solvent accumulation[9]. Although some studies have focused on understanding the interfacial mechanism, they lack a description of the dynamic variation that occurs in the interfacial solvation structure[10-12]. In view of this, it is worth exploring whether, from a dynamic perspective, the designed solvation structure can truly exert the expected effect at the interface.

Based on a representative LHCE system, we thoroughly studied the evolution of the solvation structure at the interface. As Li^+ enters the electric double layer, solvents are more inclined to enter the inner solvation sheath and replace anions, as verified by *in situ* Fourier-transform infrared spectroscopy (FTIR). In other words, a tailored anion-rich structure in bulk transforms into an anion-deficient structure at the anode interface.

In addition to revealing this unfavorable transformation, we propose a new approach for addressing the problem of anion-deficient interfaces. In a LHCE, the key diluent is usually polyfluorinated ether, which does not readily coordinate with Li^+. However,

trifluoromethoxybenzene (PhOCF$_3$) exhibits peculiar properties as a diluent. As previously reported, PhOCF$_3$ demonstrates a weaker binding ability with Li$^+$ and functions like a traditional diluent such as HFE[13-15]. Our work also reveals a unique mechanism at the electrolyte/electrode interface. ^{1}H-^{19}F heteronuclear Overhauser effect spectroscopy (HOESY) confirms that ion-dipole interactions occur between PhOCF$_3$ and anions, and that PhOCF$_3$ can, at the same time, preferentially adsorb at the LMA. This special "adsorption-attraction" mechanism can introduce more anions around the LMA, against repulsion by the electric field (**Fig. 1**). *In situ* FTIR results also show that the attenuation of the anion signal during Li$^+$ plating is less pronounced in PhOCF$_3$-LHCE than in conventional LHCE, indicating a more continuous outpouring of anions near the anode. Additionally, temperature-dependent molecular dynamics (MD) simulations and spectral characterizations reveal that the solvation structures are different at low temperatures, with fewer anions present in the inner solvation structure[16]. The solvation structure in PhOCF$_3$-LHCE demonstrates good temperature adaptivity, maintaining its anion-dominated property even at reduced temperatures.

Benefiting from the maintenance of an anion-rich solvation structure, PhOCF$_3$-LHCE enables 4.5 V Li||NCM523 cells to achieve impressive cycling performance across a wide temperature range. This work provides a dynamic perspective for enhancing cycling stability and expanding application scenarios in practical LMBs.
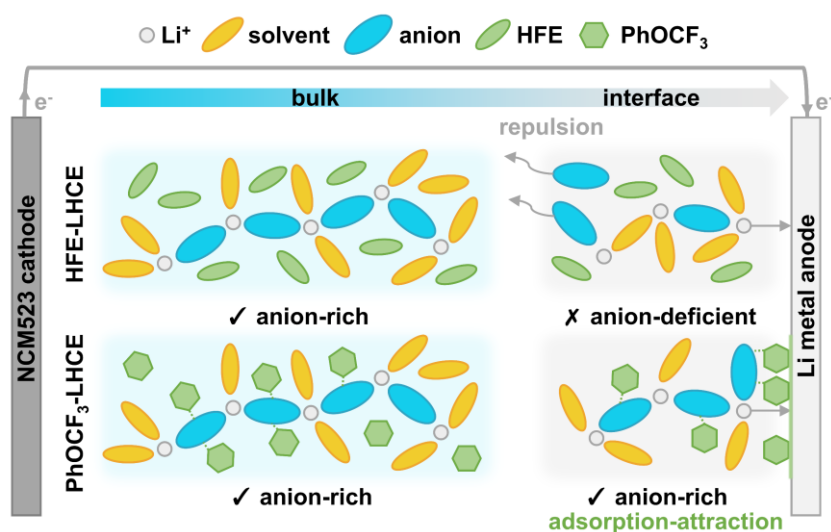
Fig. 1. Schematic illustration of the distinct anion distribution within the inner Li$^+$ solvation structure in bulk and at the LMA interface.

2. Results and discussion
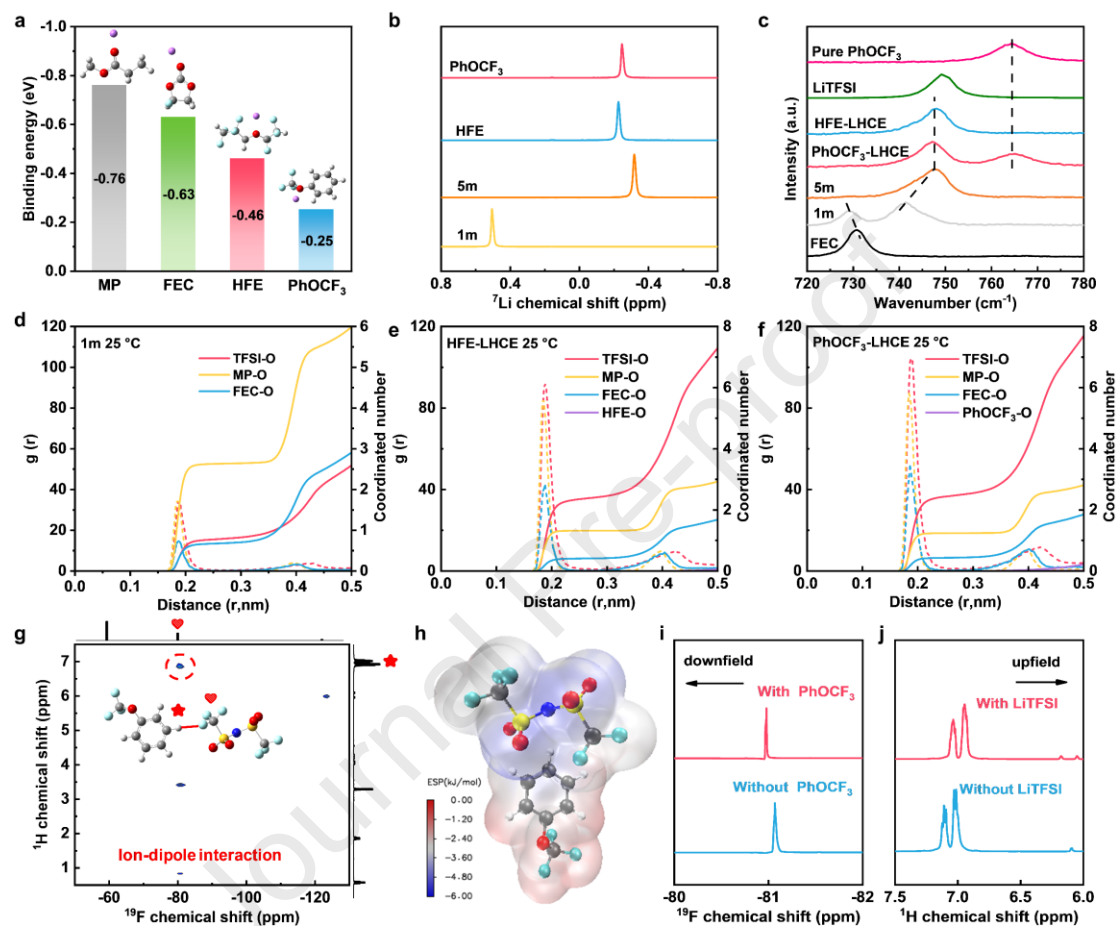
Fig. 2. (a) Binding energies of solvents with Li$^+$. (b) ^{7}Li NMR spectra of electrolytes at 25 °C. (c) Raman spectra of electrolytes at 25 °C. (d–f) The radial distribution functions (g(r), dashed lines) and coordination number (CN, solid lines) of three electrolytes at 25 °C. (g) ^{1}H-^{19}F HOESY result of PhOCF3-LHCE. (h) Binding energy of PhOCF3 solvent with TFSI$^-$. (i) ^{19}F NMR results for TFSI$^-$ in PhOCF3-LHCE with (LiTFSI in MF73 with PhOCF3) or without PhOCF3 (LiTFSI in MF73 with PhOCF3). (j) ^{1}H NMR results for PhOCF3 in PhOCF3-LHCE with (LiTFSI in MF73 with PhOCF3) or without LiTFSI (MF73 with PhOCF3).

An ideal diluent should have a weak ability to bind with Li$^+$, lower fluorine content,

and a broad liquid range to accommodate its application in a wide range of temperatures. Among various diluents, PhOCF$_3$ meets all these criteria, with a low fluorine content, broad liquid range (–50 to 102 °C), and a weak binding energy, as shown in **Fig. 2a** and **Fig. S1**. We therefore selected it as the diluent for this work. To confirm the role of PhOCF$_3$ diluent, spectral characterizations were carried out to analyze the solvation structure of different electrolytes. The ^{7}Li nuclear magnetic resonance (NMR) spectra of different electrolytes at room temperature are shown in **Fig. 2b**. As the salt concentration increases, the ^{7}Li peak shifts up-field, indicating stronger binding between Li$^+$ and TFSI$^-$. Raman spectroscopy is also an important characterization tool for analyzing the solvation structure of electrolytes. As shown in **Fig. 2c**, the wavenumber of the S-N peak in HFE-LHCE and PhOCF$_3$-LHCE is similar to that in 5m, indicating that the addition of these two diluents hardly affects the inner Li solvation sheath. MD simulations were employed to analyze the solvation structure of the electrolytes, as shown in **Figs. 2d–2f** and **Figs. S2 and S3**. In PhOCF$_3$-LHCE, the coordination number (CN) of Li$^+$ with TFSI$^-$ is around 2.4, similar to the CN in 5m and HFE-LHCE. The solvation structures of electrolytes can be classified as solvent-separated ion pairs (SSIPs), contact-ion pairs (CIPs), and aggregates (AGGs)[17]. The MD simulation results at room temperature indicate that the inner solvation sheath of PhOCF$_3$-LHCE, HFE-LHCE, and HCE is anion-rich in the bulk electrolyte (**Fig. S4** and **Tables S1–S6**), consistent with the spectral findings mentioned above.

Although the diluent hardly interacts with Li$^+$, this does not mean it cannot interact with other components of the electrolyte. Some weak interactions, such as ion-dipole and dipole-dipole, can have an important impact on the solvation structure and battery performance[18, 19]. We conducted HOESY to investigate the ion-dipole interaction between PhOCF$_3$ and TFSI$^-$. As shown in **Fig. 2g**, the H atom in the PhOCF$_3$ solvent molecule interacts with the F atom in TFSI$^-$, whereas in HFE-LHCE, a dipole-dipole interaction occurs instead, which is consistent with previous reports[20-22] (**Fig. S5**). The DFT calculations reveal that the binding energy between PhOCF$_3$ and TFSI$^-$ (–0.37 eV) is lower than that of HFE (–0.29 eV), indicating PhOCF$_3$ has a stronger anion binding affinity (**Fig. 2h** and **Fig. S6**). The NMR results confirm this affinity, as shown

in **Figs. 2i** and **2j**. The ^{1}H peak's shift towards the high field in PhOCF$_3$ after the addition of LiTFSI and the low-field shift of the ^{19}F peak in LiTFSI after the addition of PhOCF$_3$ further indicate the ion-dipole interaction between PhOCF$_3$ and LiTFSI. The ^{1}H spectra of MP and FEC exhibit a downshift after the addition of LiTFSI, suggesting these solvents interact with Li$^+$ (**Fig. S7**).
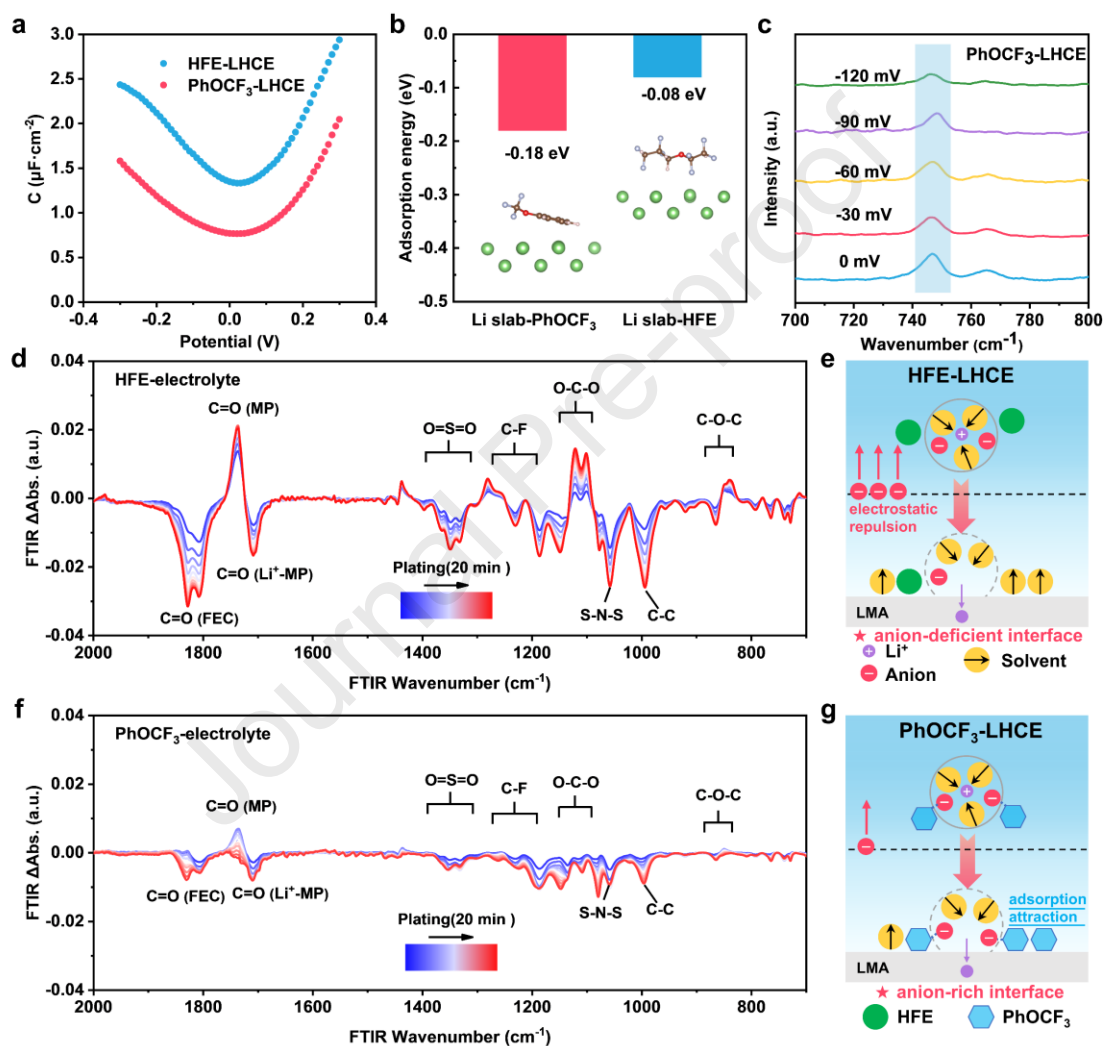
Fig. 3. (a) The differential capacitance–potential curves of Li metal from –0.3 to 0.3 V. (b) The adsorption energy of different diluents on lithium metal surface. (c) The Raman spectra on the surface of LMA in PhOCF$_3$-LHCE at various potentials. (d, f) The FTIR differential spectra of two electrolytes during the plating process. (e, g) Schematic illustrations of the desolvation process at electrolyte–electrode interface in HFE-LHCE and PhOCF$_3$-LHCE.

The adsorption behavior of PhOCF$_3$ solvent on the LMA was confirmed by differential capacitance curves, as illustrated in **Fig. 3a**. The value of PhOCF$_3$-LHCE at around 0 V is lower than that of HFE-LHCE, indicating PhOCF$_3$ adsorbs on the LMA surface and contributes to the formation of a thicker double layer[23]. In addition, there is a notable difference from the adsorption energy on the lithium metal surface, where PhOCF$_3$ exhibits a much lower adsorption energy (–0.18 eV) compared to HFE (–0.08 eV), suggesting its preferential adsorption property (**Fig. 3b**, **Fig. S8**). The "attraction-adsorption" mechanism allows PhOCF$_3$ to maintain more anions at the interface, thereby facilitating the formation of an anion-derived SEI. To confirm this, we employed *in situ* Raman characterization. In HFE-LHCE, the S–N vibration peak at 747 cm^{-1} gradually weakened as the applied polarization potential changed from 0 to –90 mV, indicating an anion-deficient interface (**Fig. S9**). In contrast, the signal of this peak was still detected at an applied potential of –120 mV in PhOCF$_3$-LHCE (**Fig. 3c**). This observation suggests that the interactions between PhOCF$_3$ and anions allow more anions to aggregate on the LMA, a mechanism absent in HFE-LHCE.

To further investigate the impact of different diluents at the interface, *in situ* FTIR spectroscopy was utilized, according to procedures described in a previous study[24]. As shown in **Fig. S10**, the peak around 996 cm^{-1} represents the C–C stretching of FEC, while the peaks at approximately 1710 and 1810 cm^{-1} correspond to the characteristic C=O vibrations of MP and FEC, respectively[25, 26]. The bands around 1060 and 1330 cm^{-1} represent the S–N–S and O=S=O vibrations of the TFSI$^-$ anion[27]. Regarding the introduced diluents, the characteristic peaks of HFE lie primarily around 1150 cm^{-1}, corresponding to C–F vibrations. For the PhOCF$_3$ solvent, the main characteristic bands are found around 1100–1250 cm^{-1}, corresponding to C–F and C–O–C stretching vibrations. Weaker benzene ring C=C stretching vibrations also occur in the 1500–1650 cm^{-1} region. From the foregoing analysis, it is clear that these characteristic peaks of the solvents and anions mentioned above do not overlap with those of the introduced HFE and PhOCF$_3$ diluents. Therefore, these peaks can be used to determine the impact of the latter two diluents during the plating process.

The FTIR spectra at the interface during the plating process in the two electrolytes are shown in **Fig. S11**. To more intuitively observe the changes in characteristic peaks at different times, the differential spectra are displayed in **Figs. 3d** and **3f**. During the plating process, the C–C stretching (996 cm^{-1}) and C=O vibration (1810 cm^{-1}) peaks assigned to FEC in the HFE-electrolyte both exhibit a downward trend. This may be due to the ring-opening decomposition of the FEC, resulting in a weakening of these characteristic peaks' intensity[28]. On the other hand, the intensity of the C=O peak (Li$^+$-MP) at 1710 cm^{-1} gradually decreases, while the intensity of the C=O peak around 1735 cm^{-1} (free MP) increases. This trend resembles previous observations and can be attributed to the desolvation process of Li$^+$, which causes coordinated solvent molecules to be expelled and form free solvent molecules. The peaks of the TFSI$^-$ corresponding to the S–N–S and O=S=O bonds both weaken during the plating process. Consequently, only a small number of anions can decompose and contribute to SEI formation, leading to a weakening of the characteristic peaks of TFSI$^-$ at the interface[29]. In contrast, the trend of PhOCF$_3$-LHCE is consistent with that of HFE-LHCE. However, due to the "adsorption-attraction" effect of PhOCF$_3$, this negative impact is suppressed. The variations of the O=S=O and S–N–S bonds are significantly reduced (**Fig. S12** and **Tables S7, S8**), and the adsorption changes for the characteristic peaks of MP solvent molecules are also diminished.

Figs. 3e and **3g** illustrate the solvation structure at the interface in HFE-LHCE and PhOCF$_3$-LHCE. Although both electrolytes possess an anion-rich solvation structure in the bulk electrolyte, the HFE-LHCE results in deficient TFSI$^-$ at the interface. In contrast, in the optimized PhOCF$_3$-LHCE, the "adsorption-attraction" effect of PhOCF$_3$ enables a greater and continuous outpouring of anions to aggregate at the electrolyte–electrode interface, triggering the formation of an anion-derived SEI rich in inorganic components.
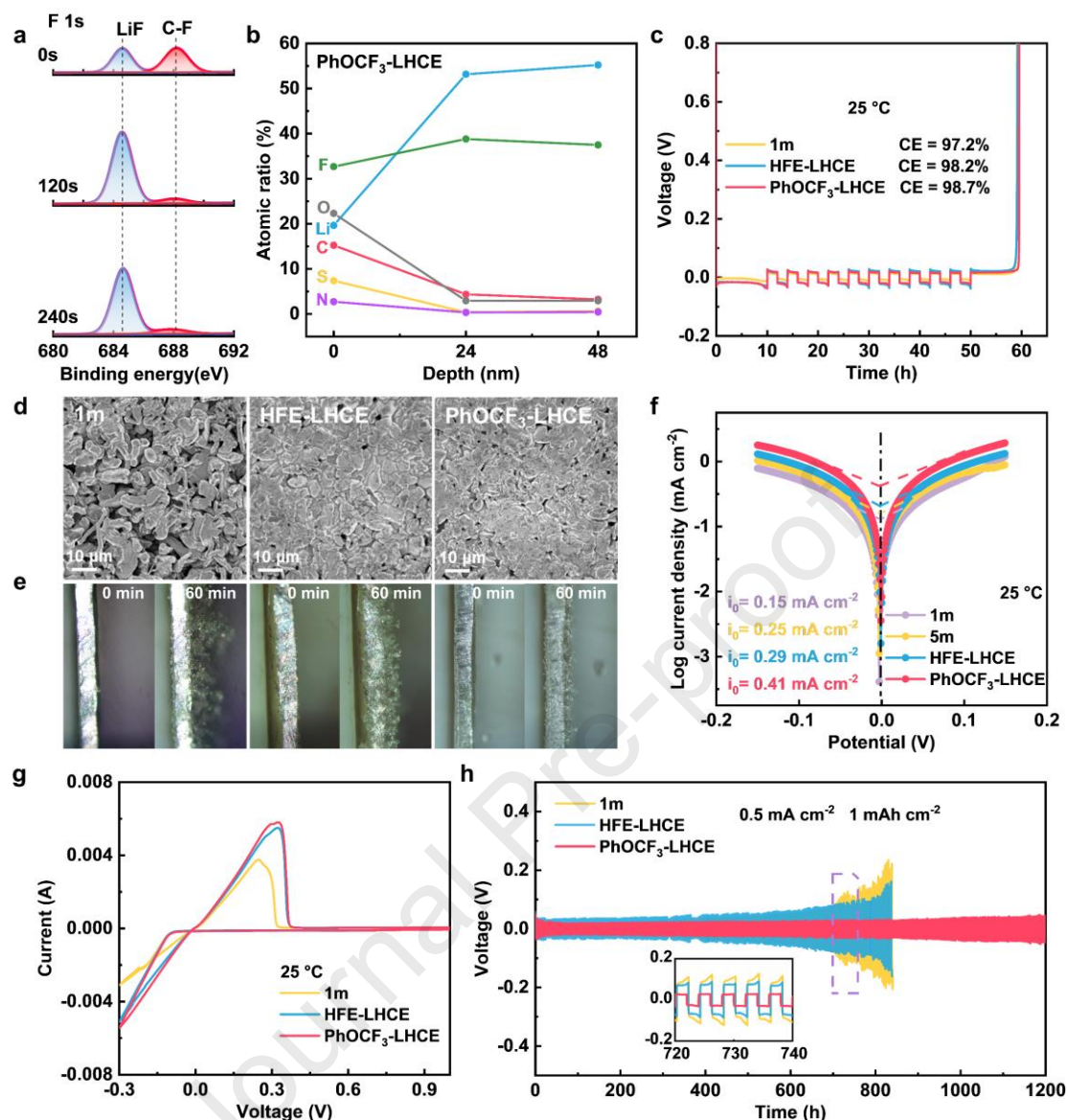
Fig. 4. (a) The F 1s spectra of SEI on cycled LMA in PhOCF₃-LHCE. (b) The atomic ratio of the SEI at various sputtering depths for PhOCF₃-LHCE. (c) The Coulombic efficiency of Li‖Cu cells with three electrolytes at 25 °C. (d) The morphology of plated Li on copper foil. (e) *In situ* optical microscope images of the Li dendrite growth process in three electrolytes. (f) Tafel curves of Li‖Li symmetric cells at 25 °C. (g) The CV results of Li‖stainless steel (SS) cells in three electrolytes at 25 °C. (h) Long-term cycling of Li‖Li cells at a current of 0.5 mA cm⁻² with a capacity of 1 mAh cm⁻².

To investigate the composition and structure of the SEI, we employed an in-depth XPS with Ar⁺ sputtering technique. The F species in **Fig. 4a** show that the content of LiF in PhOCF₃-LHCE is higher than in the other two reference electrolytes (**Fig. S13**),

indicating that PhOCF$_3$ allows more anions to approach and decompose at the anode's surface. To verify this, the various atomic ratios in the SEI at different sputtering depths are shown in **Fig. 4b** and **Fig. S14**. Before Ar$^+$ sputtering, the C element content of the SEI in HFE-LHCE and PhOCF$_3$-LHCE (10.6% and 15.2%) is lower than in 1m electrolyte (23.5%), while the F element content is higher (32.7.4% for PhOCF$_3$, 30.4% for HFE-LHCE, and 28.4% for 1m electrolyte). It is worth mentioning that although the contents of N and S elements derived from the decomposition of the anion in PhOCF$_3$-LHCE are similar to those in HFE-LHCE, analysis of the N spectra and S spectra (**Figs. S15–17**) shows that in PhOCF$_3$-LHCE, the contents of the inorganic components Li$_3$N and Li$_2$S formed by the complete decomposition of TFSI$^-$ are higher than in HFE-LHCE, which confirms that PhOCF$_3$ can promote the decomposition of anions at the interface through the "adsorption-attraction" mechanism and form an SEI rich in inorganic components. For HFE-LHCE, although the bulk has an anion-rich solvation structure, the repulsion of the interfacial electric field leads to incomplete anion decomposition, and the content of inorganic components is lower than in PhOCF$_3$, while the SEI formed in 1m electrolyte is solvent-derived and rich in organic components. In all of the electrolytes, after 120 and 240 s of sputtering, the C and O contents decrease while the Li and F contents increase. These results imply that the outer SEI is dominated by organic components (like ROCO$_2$Li, etc.), while the inner layer is primarily the inorganic component[30]. As shown in the C 1s spectra (**Fig. S18**), the C species of the SEI cycled in PhOCF$_3$-LHCE decreased with increasing depth, and its signal is lower than in 1m and HFE-LHCE. With respect to the O species in **Fig. S19**, the component at the surface of the SEI in PhOCF$_3$-LHCE is mainly composed of CO$_3$ and C=O. As the sputtering time increased, the signal of the inorganic component Li$_2$O appeared. Recent literature indicates that Li$_2$O is beneficial for improving compatibility with the LMA[31, 32]. The XPS results show that the SEI formed by PhOCF$_3$-LHCE contained more inorganic components.

To investigate the impact of an inorganic-rich SEI on the reversibility of the Li$^+$ plating/stripping process, we tested the Coulombic efficiency (CE) using Li||Cu cells. The electrolytes 1m and HFE-LHCE yielded a CE of 97.2% and 98.2%, respectively

(**Fig. 4c**). In contrast, the cells in PhOCF$_3$-LHCE achieved a higher CE of 98.7%. The morphology of the Li plated on copper foil was observed using scanning electron microscopy (SEM) (**Fig. 4d**). In 1m electrolyte, the surface is porous and broken, due to violent parasitic reactions and continuous Li dendrite growth. In HFE-LHCE, although the morphology is better, some porous areas are still observable. In contrast, the plated Li in PhOCF$_3$-LHCE exhibits a dense, uniform morphology. Additionally, as depicted in **Fig. S20**, the cells with PhOCF$_3$-LHCE exhibit a high CE of 93.8% at –20 °C, surpassing that in HFE-LHCE (91.8%) and 1m (90.4%). We also employed *in situ* optical microscopy to dynamically observe and describe the Li plating process, (**Fig. 4e**). The results showed that in the 1m electrolyte, needle-like structures appeared on the LMA's surface. In contrast, its surface in PhOCF$_3$-LHCE exhibited a relatively smooth, uniform morphology.

In terms of interfacial Li$^+$ charge transfer kinetics, the exchange current density calculated from the Tafel plot in PhOCF$_3$-LHCE (0.41 mA cm^{-2}) is higher than in other electrolytes (**Fig. 4f**). When the temperature decreases, the value is still highest in PhOCF$_3$-LHCE (**Fig. S21**). The Li||SS cell in PhOCF$_3$-LHCE also exhibits a much higher peak reduction current and larger peak area, indicating the enhanced electrochemical kinetics in PhOCF$_3$-LHCE (**Fig. 4g** and **Fig. S22**). The long-term cycling performance of the Li||Li symmetric cells using the three electrolytes is displayed in **Fig. 4h**. The cells using 1m electrolyte exhibit significant polarization, while the cells in PhOCF$_3$-LHCE demonstrate excellent stability over 1200 hours with little polarization (**Fig. S23**). In addition, the cells in PhOCF$_3$-LHCE show minimal polarization at various temperatures (**Fig. S24**) and rates (**Fig. S25**).
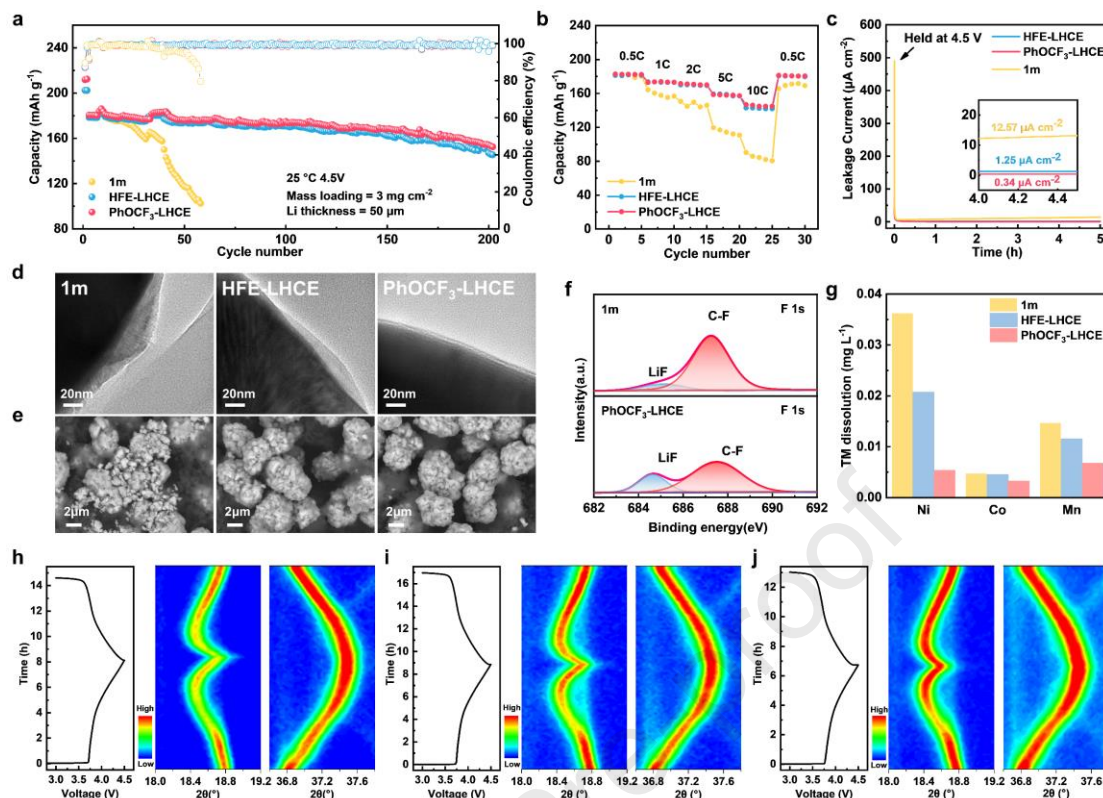
Fig. 5. (a) The cycling performance of 4.5 V Li‖NCM523 cells at a 1 C rate. (b) Rate performance of 4.5 V Li‖NCM523 cells. (c) Leakage currents of Li‖Al cells held at 5.0 V. (d, e) TEM (top) and SEM (bottom) images of NCM523 cathodes cycled in three electrolytes. (f) The F 1s spectra of NCM523 cathode cycled in 1m and PhOCF$_3$-LHCE. (g) ICP-OES analysis of LMA cycled in different electrolytes. (h–j) *In situ* XRD evolution of NCM523 cathode at the (003) and (101) diffraction peaks during the first cycle in (h) 1m, (i) HFE-LHCE, and (j) PhOCF$_3$-LHCE.

The electrochemical performance of three electrolytes was evaluated using 4.3 V Li‖NCM523 cells (**Fig. S26**). The high-loading Li‖NCM523 cells using 1m electrolyte exhibited only 59.1% capacity retention after 200 cycles, probably due to a poor SEI as well as electrolyte oxidation. When the working potential was increased to 4.5 V, the Li‖NCM523 cells with 1m electrolyte maintained a low capacity of 102.4 mAh g^{-1}, while the cells using HFE-LHCE or PhOCF$_3$-LHCE respectively delivered 144.9 mAh g^{-1} (84.6%) and 152.9 mAh g^{-1} (89.0%) capacity after 200 cycles (**Fig. 5a**). Under strict full-cell conditions of 10 mg cm^{-2} NCM523 and 50 μm Li foil, PhOCF$_3$-LHCE yielded

a capacity retention of 86.7% after 120 cycles. This performance surpassed that observed with HFE-LHCE (73.4%), as illustrated in **Fig. S27**. The enhanced electrochemical behavior of cells with PhOCF$_3$-LHCE was also corroborated by EIS results (**Fig. S28**).

As shown in **Fig. 5b**, the 4.3 V Li||NCM523 cells using 1m electrolyte delivered a capacity of 127.8 mAh g^{-1} at a 10 C rate, slightly higher than that of HFE-LHCE (122.3 mAh g^{-1}) and PhOCF$_3$ (125.6 mAh g^{-1}). Unfortunately, at 4.5 V, the cells in 1m electrolyte delivered merely 82.1 mAh g^{-1} capacity at 10 C. This was primarily due to the electrolyte's poor electrochemical stability at high voltage, as demonstrated by LSV (**Fig. S29**) and aggressive floating (**Fig. 5c** and **Fig. S30**) tests. Although the cells in HFE-LHCE retained a capacity of 141.9 mAh g^{-1} at 10 C, that was still lower than in PhOCF$_3$-LHCE (144.9 mAh g^{-1}), primarily due to the former's relatively sluggish desolvation process (**Fig. S31**) and wettability with the separator (**Fig. S32**).

TEM images of the cycled cathodes are displayed in **Fig. 5d**. When 1m electrolyte was used, the CEI appears thick and uneven, failing to protect the cathode from side reactions at high voltage. In the case of HFE-LHCE, although the CEI is thinner, its surface remains a little uneven. In stark contrast, a thin, uniform CEI is observed on the cathode surface in PhOCF$_3$-LHCE, effectively mitigating parasitic reactions and contributing to better electrochemical performance. In addition, as shown in **Fig. 5e**, the SEM images of NCM523 particles cycled in 1m electrolyte appear broken and full of cracks. In contrast, particles cycled in HFE-LHCE and PhOCF$_3$-LHCE remain as intact as pristine ones (**Fig. S33**). To identify the primary factor contributing to the enhancement, we carried out XPS to analyze the CEI's chemical components (**Fig. 5f** and **Fig. S34**). Similar to the SEI, the CEI formed in HFE-LHCE is rich in inorganic components such as LiF and Li$_2$CO$_3$, which are derived from anion decomposition. The CEI in PhOCF$_3$-LHCE also exhibits a higher proportion of inorganic materials, indicating that using PhOCF$_3$ diluent can also achieve this positive effect. By comparison, the CEI formed in 1m electrolyte is predominantly composed of organic species originating from the decomposition of solvents.

The dissolution of transition metal ions (TMi) is a significant factor contributing to

a cell's performance degradation, not only disrupting the cathode's structure but also negatively affecting the SEI[33]. The TMi content was quantified using inductively coupled plasma optical emission spectroscopy (ICP-OES) (**Fig. 5g** and **Table S9**), which showed that the TMi content in PhOCF₃-LHCE was notably lower than in the other two reference electrolytes; this is attributed to the robust CEI formed in PhOCF₃-LHCE. *In situ* XRD was employed to assess the cathode's structural evolution during cycling. In the charging process, the (003) peak first shifts left and then right, while the (101) peak moves to the right. These variations in the (003) and (101) peaks are closely related to the lattice expansion/contraction process[34, 35]. The NCM523 cathode cycled in PhOCF₃-LHCE (**Fig. 5h**) exhibits more reversible changes compared to those in 1m (**Fig. 5i**) and HFE-LHCE (**Fig. 5j**). Detail information on the variations in lattice parameters is provided in **Table S10**. The volume variation of NCM523 in PhOCF₃-LHCE was 0.09%, better than in 1m (0.27%) and HFE-LHCE (0.17%), which led to lower resistance and facilitated faster Li^+ transport[36] (**Fig. S35**). These results suggest NCM523 had better structural stability in PhOCF₃-LHCE during cycling, explaining its excellent long-term cycling performance.
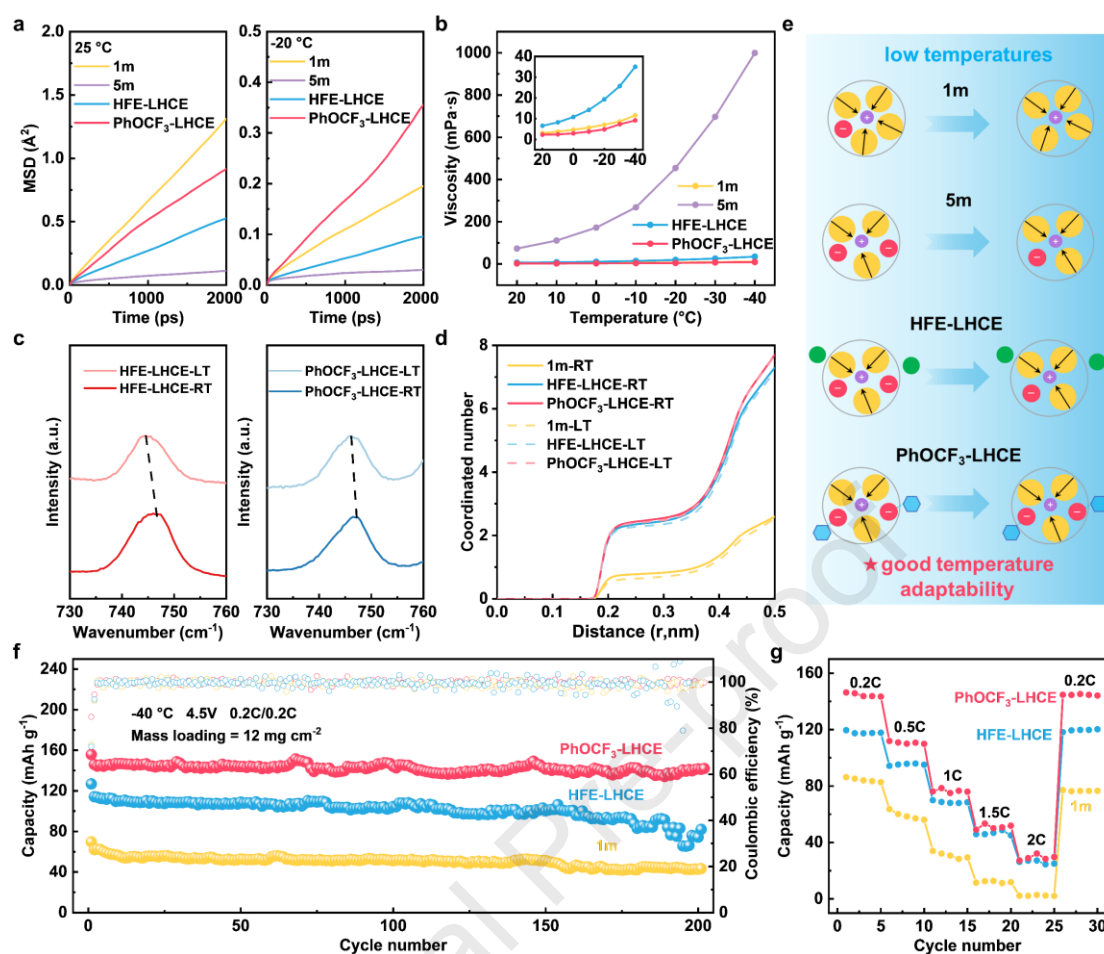
Fig. 6. (a) MSD plots in three electrolytes at room and low temperatures. (b) The viscosity of electrolytes at various temperatures. (c) Temperature-dependent Raman spectra. (d) The CN of TFSI$^-$ anions in all electrolytes at different temperatures. (e) A schematic illustration of temperature adaptivity in three electrolytes. (f) The charge/discharge cycling performance of Li||NCM523 in three electrolytes at –40 °C and 0.2 C. (g) The rate performance of 4.5 V Li||NCM523 cells at –40 °C.

The performance of LMBs deteriorates much faster at low temperatures due to slow bulk Li$^+$ diffusion and impeded charge transfer kinetics. To evaluate the transport capability of the electrolytes, we calculated their diffusion coefficients based on the mean square displacement (MSD) results (**Fig. 6a** and **Table S11**). At 25 °C, the diffusion coefficient of 1m is highest among the electrolytes, but at –20 °C, the diffusion coefficient of PhOCF$_3$-LHCE surpasses that of 1m, indicating the former's faster Li$^+$ transportation in bulk electrolyte at a low temperature. These results are corroborated

by viscosity measurements (**Fig. 6b**). Notably, the viscosity of 5m electrolyte increases significantly as the temperature decreases, reaching approximately 1000 mPa·s at – 40 °C. However, with the introduction of the diluents, the viscosity decreases notably. The viscosity of PhOCF$_3$-LHCE is lower than that of 1m, measuring only 9.2 mPa·s at –40 °C. As illustrated in **Fig. S36**, the conductivities of 5m, HFE-LHCE, and PhOCF$_3$-LHCE are relatively similar at 20 °C. However, at low temperatures, PhOCF$_3$-LHCE begins to outperform the other two electrolytes in terms of conductivity. This may be ascribed to the low viscosity of PhOCF$_3$-LHCE, which facilitates Li$^+$ transport in the bulk electrolyte[37]. The Li$^+$ transference number of PhOCF$_3$-LHCE is also higher than those of other electrolytes (**Fig. S37**).

The desolvation process at the interface plays a crucial role in cells' performance at low temperatures[38, 39]. Although the solvation structure of LHCE exhibits many advantages, it changes at low temperatures, so we conducted temperature-dependent spectral characterizations. As shown in **Fig. 6c** and **Fig. S38**, the S-N vibration peak of PhOCF$_3$-LHCE is less pronounced than for other electrolytes, a trend confirmed by temperature-dependent NMR (**Fig. S39**) and MD simulations (**Figs. S40–42**). As the simulation temperature decreases from 25 to –20 °C, there is no significant change in the CN of Li$^+$ with TFSI$^-$ in PhOCF$_3$-LHCE (**Fig. 6d**). However, in 1m electrolyte, the CN decreases from 0.8 to 0.6. The detailed data are available in **Tables S12–17**. Analysis of these findings showed that the PhOCF$_3$-LHCE not only exhibits traditional LHCE's anion-dominated solvation structure but also demonstrates better temperature-adaptivity with respect to maintaining the solvation structure (**Fig. 6e**).

High-loading Li‖NCM523 cells with PhOCF$_3$-LHCE retained a capacity of 142.0 mAh g^{-1} after 200 cycles at 0.2 C, surpassing the other two electrolytes' performance (**Fig. 6f**). This difference was confirmed by low-temperature *in situ* EIS results (**Fig. S43**). Furthermore, the rate performance results in **Fig. 6g** show that cells in PhOCF$_3$-LHCE can operate at 2 C even at –40 °C. The PhOCF$_3$-LHCE also yielded excellent discharge performance even at –70 °C (**Fig. S44**). The above results demonstrate that the addition of PhOCF$_3$ diluent can preserve the benefits of the anion-dominated solvation structure even at reduced temperatures, promoting the transport of Li$^+$ in both

the bulk and the interface. This contributes to the cells' enhanced low-temperature performance.

3. Conclusion

In summary, this work has used several characterization techniques and methods to identify variations in the solvation structure in terms of the interface. When approaching the interface, the solvation structure of Li^+ tends to become anion-deficient, which is unfavorable for the desolvation process and the formation of an anion-derived SEI, thereby resulting in electrochemical performance degradation. The PhOCF$_3$-LHCE electrolyte designed in this work can suppress these unfavorable changes. The preferential adsorption of PhOCF$_3$ on the LMA and its ion-dipole interaction with anions can maintain more anions around the LMA by means of the adsorption-attraction mechanism. This mechanism takes advantage of the positive effects of the solvation structure at the interface, similar to the solvation structure in the bulk electrolyte. The results from temperature-dependent MD and spectral characterizations reveal that the solvation structure of PhOCF$_3$-LHCE demonstrates good temperature adaptivity under low-temperature conditions. These properties enable 4.5 V Li||NCM523 full cells to deliver a capacity of 142.0 mAh g^{-1} after 200 cycles at -40 °C. This work offers in-depth insights into the evolution of the solvation structure of electrolytes during cycling and presents an effective strategy for designing electrolytes that can be used in practical LMBs.

calculations in this paper were done at Hefei Advanced Computing Center.

Conflict of Interest

The authors declare no conflict of interest.

References

[1] W. Xu, J. Wang, F. Ding, X. Chen, E. Nasybulin, Y. Zhang, J.G. Zhang, Lithium metal anodes for rechargeable batteries. Energy Environ. Sci. 7 (2014) 513-537.

[2] P. Albertus, S. Babinec, S. Litzelman, A. Newman, Status and challenges in enabling the lithium metal electrode for high-energy and low-cost rechargeable batteries. Nat. Energy 3 (2017) 16-21.

[3] D.H. Liu, Z. Bai, M. Li, A. Yu, D. Luo, W. Liu, L. Yang, J. Lu, K. Amine, Z. Chen, Developing high safety Li-metal anodes for future high-energy Li-metal batteries: strategies and perspectives. Chem. Soc. Rev. 49 (2020) 5407-5445.

[4] Y. Yamada, K. Furukawa, K. Sodeyama, K. Kikuchi, M. Yaegashi, Y. Tateyama, A. Yamada, Unusual stability of acetonitrile-based superconcentrated electrolytes for fast-charging lithium-ion batteries. J. Am. Chem. Soc. 136 (2014) 5039-5046.

[5] J. Holoubek, K. Kim, Y. Yin, Z. Wu, H. Liu, M. Li, A. Chen, H. Gao, G. Cai, T.A. Pascal, P. Liu, Z. Chen, Electrolyte design implications of ion-pairing in low-temperature Li metal batteries. Energy Environ. Sci. 15 (2022) 1647-1658.

[6] Y.X. Yao, X. Chen, C. Yan, X.Q. Zhang, W.L. Cai, J.Q. Huang, Q. Zhang, Regulating interfacial chemistry in lithium-ion batteries by a weakly solvating electrolyte. Angew. Chem. Int. Ed. 60 (2021) 4090-4097.

[7] J. Holoubek, H. Liu, Z. Wu, Y. Yin, X. Xing, G. Cai, S. Yu, H. Zhou, T.A. Pascal, Z. Chen, P. Liu, Tailoring electrolyte solvation for Li metal batteries cycled at ultra-low temperature. Nat. Energy 6 (2021) 303-313.

[8] Y. Yang, W. Yang, H. Yang, H. Zhou, Electrolyte design principles for low-temperature lithium-ion batteries. eScience 3 (2023) 100170.

[9] J. Wang, J. Luo, H. Wu, X. Yu, X. Wu, Z. Li, H. Luo, H. Zhang, Y. Hong, Y. Zou, S. Cao, Y. Qiao, S.G. Sun, Visualizing and regulating dynamic evolution of interfacial electrolyte configuration

during de-solvation process on lithium-metal anode. Angew. Chem. Int. Ed. 63 (2024) e202400254.

[10] M. Qin, Z. Zeng, X. Liu, Y. Wu, R. He, W. Zhong, S. Cheng, J. Xie, Revealing surfactant effect of trifluoromethylbenzene in medium-concentrated PC electrolyte for advanced lithium-ion batteries. Adv. Sci. 10 (2023) e2206648.

[11] Y.Y. Wang, J.K. Gu, B.H. Zhang, G.R. Li, S. Liu, X.P. Gao, Specific adsorption reinforced interface enabling stable lithium metal electrode. Adv. Funct. Mater. 32 (2022) 202112005.

[12] M. Yang, K. Chen, H. Li, Y. Cao, H. Yang, X. Ai, Molecular adsorption-induced interfacial solvation regulation to stabilize graphite anode in ethylene carbonate-free electrolytes. Adv. Funct. Mater. 33 (2023) 202306828.

[13] C. Li, Y. Li, Y. Wang, F. Bai, X. Chen, T. Li, Developing diluted low-concentration electrolyte with a high anion-to-solvent ratio for high-voltage lithium metal batteries. J. Mater. Chem. A 12 (2024) 8236-8243.

[14] X. Liu, A. Mariani, T. Diemant, M.E. Di Pietro, X. Dong, A. Mele, S. Passerini, Reinforcing the electrode/electrolyte interphases of lithium metal batteries employing locally concentrated ionic liquid electrolytes. Adv. Mater. 36 (2024) e2309062.

[15] C. Zhu, C. Sun, R. Li, S. Weng, L. Fan, X. Wang, L. Chen, M. Noked, X. Fan, Anion–diluent pairing for stable high-energy Li metal batteries. ACS Energy Lett. 7 (2022) 1338-1347.

[16] P. Lai, Y. Zhang, B. Huang, X. Deng, H. Hua, Q. Chen, S. Zhao, J. Dai, P. Zhang, J. Zhao, Revealing the evolution of solvation structure in low-temperature electrolytes for lithium batteries. Energy Stor. Mater. 67 (2024) 103314.

[17] Y. Wang, Z. Li, Y. Hou, Z. Hao, Q. Zhang, Y. Ni, Y. Lu, Z. Yan, K. Zhang, Q. Zhao, F. Li, J. Chen, Emerging electrolytes with fluorinated solvents for rechargeable lithium-based batteries. Chem. Soc. Rev. 52 (2023) 2713-2763.

[18] T. Cai, Y. Wang, F. Zhao, Z. Ma, P. Kumar, H. Xie, C. Sun, J. Wang, Q. Li, Y. Guo, J. Ming, Graphic, quantitation, visualization, standardization, digitization, and intelligence of electrolyte and electrolyte-electrode interface. Adv. Energy Mater. 14 (2024) 2400569.

[19] Y. Zou, Z. Ma, G. Liu, Q. Li, D. Yin, X. Shi, Z. Cao, Z. Tian, H. Kim, Y. Guo, C. Sun, L. Cavallo, L. Wang, H.N. Alshareef, Y.K. Sun, J. Ming, Non-flammable electrolyte enables high-voltage and wide-temperature lithium-ion batteries with fast charging. Angew. Chem. Int. Ed. 62 (2023) e202216189.

[20] H. Liang, Z. Ma, Y. Wang, F. Zhao, Z. Cao, L. Cavallo, Q. Li, J. Ming, Solvent-solvent interaction mediated lithium-ion (fe)intercalation chemistry in propylene carbonate based electrolytes for lithium-sulfur batteries. ACS Nano 17 (2023) 18062-18073.

[21] Y. Wang, Z. Cao, Z. Ma, G. Liu, H. Cheng, Y. Zou, L. Cavallo, Q. Li, J. Ming, Weak solvent–solvent interaction enables high stability of battery electrolyte. ACS Energy Lett. 8 (2023) 1477-1484.

[22] Y. Wang, Z. Cao, W. Wahyudi, Z. Ma, Y. Liang, L. Cavallo, Q. Li, J. Ming, Electrolyte-mediated misconception of carbon-based electrode performance and beyond in metal-ion batteries. Adv. Energy Mater. 13 (2023) 2301354.

[23] R. Jia, H. Dai, X. Tu, C. Sun, S. Sun, C. Lai, Hexabutylcyclohexane-1,2,3,4,5,6-hexaimine additive-assisted commercial ester electrolyte for 4.7 V highly-stable Li metal batteries. Adv. Energy Mater. 13 (2023) 2302747.

[24] X. Yu, M. Chen, Z. Li, X. Tan, H. Zhang, J. Wang, Y. Tang, J. Xu, W. Yin, Y. Yang, D. Chao, F. Wang, Y. Zou, G. Feng, Y. Qiao, H. Zhou, S.G. Sun, Unlocking dynamic solvation chemistry and hydrogen evolution mechanism in aqueous zinc batteries. J. Am. Chem. Soc. 146 (2024) 17103-17113.

[25] Y. Akita, M. Segawa, H. Munakata, K. Kanamura, In-situ fourier transform infrared spectroscopic analysis on dynamic behavior of electrolyte solution on $LiFePO_4$ cathode. J. Power Sources 239 (2013) 175-180.

[26] T. Hou, G. Yang, N. Rajput, J. Self, S. Park, J. Nanda, K. Persson, The influence of FEC on the solvation structure and reduction reaction of $LiPF_6$/EC electrolytes and its implication for solid electrolyte interphase formation. Nano Energy 64 (2019) 103881.

[27] L. Wu, J. Hu, S. Chen, X. Yang, L. Liu, J.S. Foord, P. Pobedinskas, K. Haenen, H. Hou, J. Yang, Lithium nitrate mediated dynamic formation of solid electrolyte interphase revealed by in situ Fourier transform infrared spectroscopy. Electrochim. Acta 466 (2023) 142973.

[28] D. Liu, K. Qian, Y.-B. He, D. Luo, H. Li, M. Wu, F. Kang, B. Li, Positive film-forming effect of fluoroethylene carbonate (FEC) on high-voltage cycling with three-electrode $LiCoO_2$/Graphite pouch cell. Electrochim. Acta 269 (2018) 378-387.

[29] V. Rikka, S. Sahu, A. Chatterjee, P. Satyam, R. Prakash, M. Rao, R. Gopalan, G. Sundararajan, In situ/ex situ investigations on the formation of the mosaic solid electrolyte interface layer on graphite anode for lithium-ion batteries. J. Phys. Chem. C 122 (2018) 28717-28726.

[30] E. Peled, S. Menkin, Review—SEI: past, present and future. J. Electrochem. Soc., 164 (2017) A1703.

[31] G.M. Hobold, C. Wang, K. Steinberg, Y. Li, B.M. Gallant, High lithium oxide prevalence in the lithium solid–electrolyte interphase for high Coulombic efficiency. Nat. Energy 9 (2024) 580–591.

[32] H. Zeng, K. Yu, J. Li, M. Yuan, J. Wang, Q. Wang, A. Lai, Y. Jiang, X. Yan, G. Zhang, H. Xu, J. Wang, W. Huang, C. Wang, Y. Deng, S.S. Chi, Beyond LiF: tailoring Li_2O-dominated solid electrolyte interphase for stable lithium metal batteries. ACS Nano 18 (2024) 1969-1981.

[33] Z. Piao, X. Wu, H.-R. Ren, G. Lu, R. Gao, G. Zhou, H.-M. Cheng, A semisolvated sole-solvent electrolyte for high-voltage lithium metal batteries. J. Am. Chem. Soc. 145 (2023) 24260-24271.

[34] J. Shu, R. Ma, L. Shao, M. Shui, K. Wu, M. Lao, D. Wang, N. Long, Y. Ren, In-situ X-ray diffraction study on the structural evolutions of $LiNi_{0.5}Co_{0.3}Mn_{0.2}O_2$ in different working potential windows. J. Power Sources 245 (2014) 7-18.

[35] D. Zhang, M. Liu, J. Ma, K. Yang, Z. Chen, K. Li, C. Zhang, Y. Wei, M. Zhou, P. Wang, Y. He, W. Lv, Q.-H. Yang, F. Kang, Y. He, Lithium hexamethyldisilazide as electrolyte additive for efficient cycling of high-voltage non-aqueous lithium metal batteries. Nat. Commun. 13 (2022) 6966.

[36] J. Liu, J. Wang, Y. Ni, J. Liu, Y. Zhang, Y. Lu, Z. Yan, K. Zhang, Q. Zhao, F. Cheng, J. Chen, Tuning interphase chemistry to stabilize high-voltage $LiCoO_2$ cathode material via spinel coating. Angew. Chem. Int. Ed. 61 (2022) e202207000.

[37] P. Lai, X. Deng, Y. Zhang, J. Li, H. Hua, B. Huang, P. Zhang, J. Zhao, Bifunctional localized high-concentration electrolyte for the fast kinetics of lithium batteries at low temperatures. ACS Appl. Mater. Interfaces 15 (2023) 31020-31031.

[38] Q. Li, D. Lu, J. Zheng, S. Jiao, L. Luo, C.M. Wang, K. Xu, J.G. Zhang, W. Xu, Li^+-desolvation dictating lithium-ion battery's low-temperature performances. ACS Appl. Mater. Interfaces 9 (2017) 42761-42768.

[39] K. Xu, "Charge-Transfer" process at graphite/electrolyte interface and the solvation sheath structure of Li^+ in nonaqueous electrolytes. J. Electrochem. Soc. 154 (2007) A162.

Highlights

1. 2D NMR HOESY reveals implicit ion-dipole interactions between $PhOCF_3$ and anions.

2. An "adsorption-attraction" mechanism for $PhOCF_3$-LHCE at the interface is proposed.

3. Temperature-dependent solvation structures are studied using molecular dynamics and spectral methods.

4. Stable cycling of 4.5 V Li||NCM523 cells containing $PhOCF_3$-LHCE is achieved over a wide temperature range.

Declaration of interests

☒ The authors declare that they have no known competing financial interests or personal

relationships that could have appeared to influence the work reported in this paper.

☐The authors declare the following financial interests/personal relationships which may be

considered as potential competing interests: